Letter Vol. 5, No. 2 / February 2018 / Optica 204

Scatterer recognition via analysis of speckle patterns

Eadan Valent and Yaron Silberberg*

Department of Physics of Complex Systems, Weizmann Institute of Science, Rehovot 76100, Israel
**Corresponding author: yaron.silberberg@weizmann.ac.il*

Received 5 December 2017; revised 11 January 2018; accepted 12 January 2018 (Doc. ID 314240); published 14 February 2018

Light scattering due to interaction with a material has long been known to create speckle patterns. We have demonstrated that even though speckle patterns from different objects are very similar, they contain minute dissimilarities that can be used to differentiate between the originating scatterers. We first approached this problem using a convolutional neural network—a deep learning algorithm—to show that indeed specific speckle patterns can be linked to the respective materials creating them. We then progressed to use recorded speckle patterns created from different materials in order to measure statistical parameters that possess a well-defined physical meaning. Using these parameters gave similar scatterer recognition abilities while gaining insight on the physical reasons for these material-dependent statistical deviations.

OCIS codes: (290.0290) Scattering; (030.6140) Speckle; (030.6600) Statistical optics; (070.5010) Pattern recognition.

https://doi.org/10.1364/OPTICA.5.000204

Optical speckle patterns were first observed in the early 1960s when laser light was reflected from rough surfaces and have since been studied and applied extensively [1,2]. Speckles are formed from the summation of many field components that arrive at the observation screen from different points on the scattering object, each with a random phase and amplitude. For numerous purposes, speckles are viewed as a burden and are commonly suppressed [3]. On the other hand, speckles have been exploited to reconstruct an object that cannot be directly observed [4] and for speckle interferometry [5] and microscopy [6]. Additionally, several techniques using speckles to study the roughness of an object's surface have been demonstrated [7] that rely on mathematical models that assume no volumetric scattering [8], some even utilizing machine learning [9].

In their simplest description, speckles are analyzed as a random addition of scalar fields. They are then predicted to exhibit Gaussian amplitude statistics, which are responsible for some of the commonly observed features—contrast and correlations [1]. Since speckles are usually observed in the far field, there is a reversal of scales: the small features of the scattering object are responsible for the larger features in the speckle field, and vice versa—the individual speckle shapes and sizes are determined by the intensity envelope of the light as it exits the medium. Since the speckles themselves are less sensitive to the fine details of the scattering object, one may wonder if a subsection of a speckle field contains any information about the particular scattering object. This is the main question we address in this current work.

To investigate this point, we collected data by illuminating different scattering materials with the same identical light source and measuring their respective scattered speckles. Using a machine-learning algorithm—specifically, the convolutional neural network (CNN) algorithm [10]—we found that we were able to teach the algorithm to successfully classify different scattering objects based on their far-field speckle pattern. This affirmed that some information in the speckle pattern is indeed material specific, yet gave no insight on what those features might be. Therefore, we moved on to creating a linear discriminant analysis (LDA) algorithm [11] that uses statistical parameters of the speckle field for the same purpose, in an attempt to apprehend the source of these material-specific deviations.

There have been many mathematical models developed to describe the speckle patterns resulting from the interaction of light with diffusers possessing specific statistical features [1]. These models are quite straightforward for thin diffusers (single scattering events), either in reflection or in transmission, but less so for the thick diffuser regime, where multiple scattering adds to the complexity. When looking at light scattered from a thin diffuser, the amplitude envelope and light polarization remain practically unchanged and only the phase is affected. On the other hand, when light undergoes multiple scattering in thick diffusers, both the amplitude envelope and directionality are distorted and the field's original polarization is lost. These deformations are specific to the diffuser at hand and affect the speckle pattern created in the far field in two ways. The light's loss of original polarization in the diffuser affects the speckle pattern's contrast. Thus, when a light source with a well-defined polarization illuminates a diffuser, the outgoing pattern's contrast depends on what proportion of the light changed polarization. Multiple scattering in thick diffusers also affects the shape of the field that emerges from the medium, and since the individual speckle shape is determined by the amplitude envelope of the field immediately as it exits the diffuser, we expect the autocorrelation function of the speckle pattern to contain information that is both surface and medium specific.

In the case of a fully developed polarized speckle pattern, as created by thin diffusers, the expected second moment of the intensity is [1]

$$\langle I^2 \rangle = 2\langle I \rangle^2. \tag{1}$$

Contrarily, light scattered from thick diffusers is no longer polarized, and can therefore be modeled as a sum of two speckle patterns with orthogonal polarizations with the total intensity being an incoherent sum of the two fields: $I = I_x + I_y$. The ratio between the intensities in each polarization can be defined as $\eta = I_y/I_x$, where I_y is the smaller component. Assuming uncorrelated intensity patterns, each being a fully developed speckle pattern, the expected contrast is [1]

$$C = \sqrt{1+\eta^2}/(1+\eta). \tag{2}$$

This continuous range of the contrast is material dependent and will be one of the fingerprints for scatterer recognition. The amount of polarization mixing depends on the probabilities of the different paths the light can undertake within the medium. These paths are dictated by the material thickness and its scattering features, such as the linear absorption coefficient, the linear scattering coefficient, and the asymmetry coefficient.

In order to capture the effect of amplitude envelope distortion within a diffuser, a derivation from the Van Cittert–Zernike theorem [1] can be used, assuming the illumination spot size is much larger than the correlation area of the scatterer at hand. This formula provides a way to deduce the amplitude envelope of the scattered field as it exits the medium by measuring the autocorrelation of the speckle pattern's intensity in the far field,

$$\Gamma_I(\Delta x,\Delta y) = \bar{I}^2\left[1+\left|\frac{\iint I(\alpha,\beta)\exp\left(-i\frac{2\pi}{\lambda z}[\alpha\Delta x+\beta\Delta y]\right)\mathrm{d}\alpha\mathrm{d}\beta}{\iint I(\alpha,\beta)\mathrm{d}\alpha\mathrm{d}\beta}\right|^2\right], \tag{3}$$

where $[\alpha,\beta]$—coordinates in the scatterer plane, $[x,y]$—coordinate in the observer plane. Alternately, we can consider the power spectral density function by performing a 2D Fourier transformation on $\Gamma_I(\Delta x,\Delta y)$,

$$G_I(u_x,u_y) = \bar{I}^2\left[\delta(u_x,u_y)+\frac{\iint I(\alpha,\beta)I(\alpha+\lambda z u_x,\beta+\lambda z u_y)\mathrm{d}\alpha\mathrm{d}\beta}{[\iint I(\alpha,\beta)\mathrm{d}\alpha\mathrm{d}\beta]^2}\right]. \tag{4}$$

Both of these functions are sensitive to wavefront distortions caused to the light source within a specific diffuser. We used G_I as our second fingerprint for scatterer recognition. The relative amount of smearing to our input beam's amplitude envelope due to the diffuser depends on the material's scattering features, thickness, and the input beam's size and directionality in relation to the material surface.

The setup, shown schematically in Fig. 1, had an option for both transmission and reflection measurements. A continuous-wave single-mode linearly polarized He–Ne laser ($\lambda = 632.8$ nm; 30 mW; Melles Griot) with a Gaussian amplitude profile and a beam width of ~1 mm was used as the light source. In the reflection case, the laser was pointed 2.5 cm below the center of a motorized rotational stage (ThorLabs) with a connected mount for the tested materials to be attached to. This assured that the scattering plane was always in the same location and angle in respect to the laser. A CMOS camera (Flea3, PointGrey) with an optional polarizer was placed at a distance of 21 cm and an angle of 6° in respect to the laser axis and was used to detect the outgoing speckle pattern. This assured that the observation plane was consistent for all measurements and that minimal specular back-reflected light be received. The camera distance from the material was chosen to be in the far field for all materials tested with individual speckles covering roughly twenty by twenty pixels for the average material tested. The rotational stage was used to shift the object and collect many (180) distinct patterns of a material without having to move the laser beam and without affecting its directionality and position in the scattering plane. Care was taken to ensure that the stage and sample were stationary in each exposure. Also, at the beginning of every measurement, the shutter time of the camera was adjusted such that all data collected would have a similar mean intensity. This utilizes the full dynamic range of the camera to achieve maximal resolution and simultaneously ensures a consistent noise level for all measurements.

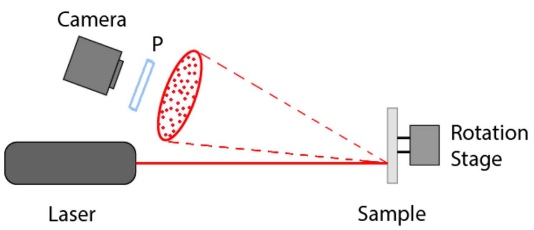

Fig. 1. Experimental setup: He–Ne laser beam is pointed at the scattering sample. The sample emits speckles in all directions and the cameras detect a small subsection of this pattern. A polarizer (P) may be placed on the cameras to only view a desired polarization.

The same setup was used also for transmission measurements, except that a set of mirrors redirected the input light beam around and through the stage and illuminated the sample on its rear side through a hole in the mount. The light was directed back towards the original laser axis to ensure that the ballistic light that does not interact with the material sample will not reach the camera.

In both cases, we recorded speckle images with and without a polarizer in front of the camera. Also, when possible, we varied the thickness of the medium and tested the effect of thickness on the resulting speckle field.

After collecting N speckle images from each scatterer in each polarization, we extract statistical parameters for each image (detailed in Supplement 1) and save both the entire image and its measured "parameter vector." We then group the M different data sets (different materials in a particular polarization), insert them into an algorithm, and check its recognition capability. Two machine-learning algorithms were used in this work. The first is a CNN algorithm that uses raw speckle images as inputs. The other is an LDA algorithm that uses the parameter vectors as inputs. Both algorithms first normalize each image's intensity in order to rule out the option that we are simply sensitive to the material's reflectivity.

As previously mentioned, the CNN algorithm starts with the raw speckle patterns as recorded by the camera, and after a training session with sets of two or more families of scatterers, it was able to classify a new speckle pattern into one of these families. The results are shown in Fig. 2(a). Each group presents results from a particular family of scatterers (see caption for details), while each color bar represents a different polarization measurement—without a polarizer and with polarizations parallel and perpendicular to the illumination. Given a single new speckle pattern (single-shot mode), the algorithm was able to successfully identify the correct material around 70% of the time, even when the materials were very similar and the patterns appeared indistinguishable to the human eye. This result proves that there are small yet distinct differences between the speckles produced by similar materials, although it does not point to the origin of these differences.

To look further into this point, we calculated the average speckle autocorrelation function produced by different materials

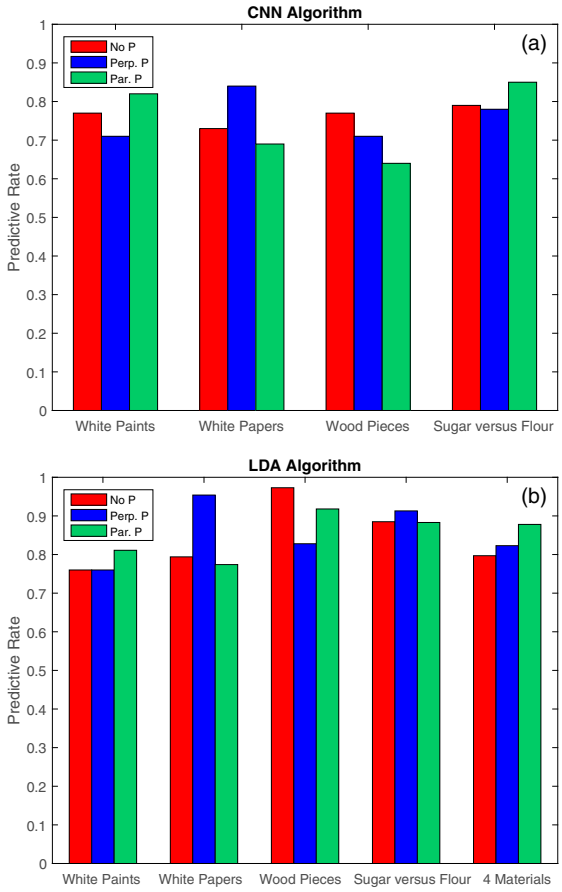

Fig. 2. Predictive rates for several material sets. Data collected in single shot mode with: no polarizer, polarizer perpendicular to illumination, and parallel to illumination. (a) CNN algorithm. (b) LDA algorithm. White paints: two slabs of the same paint, dried with different surface roughness levels. White paper stacks: paper from two different manufacturers. Wood: Two pieces of different plywood. Powdered sugar and flour were encased in a petri dish. Four material set: slab of white paint, white plastic, wood, and white paper. Error bars are not presented since the errors are <1% in the LDA case (see Supplement 1) and ambiguous in the CNN case.

in the backscattered case [Figs. 3(a) and 3(b)]. There are small yet clear differences in the autocorrelation shape for each material, resulting from the different speckle shapes/sizes and pattern contrast. Since the average speckle shape (and hence its autocorrelation) depends on the light as it emerges from the scatterer, and since we have taken care to keep the illumination geometry fixed, we attribute these differences to distortions of the outgoing light profile due to the scatterer's surface and the light diffusion that occurred inside of the medium. These distortions are sensitive to the materials' scattering parameters; hence, using the speckles' autocorrelation may be used as a convenient measure to learn about materials.

The peak heights for the polarized case [Fig. 3(a)] do not reach the value 2 [as expected from Eq. (1)], probably due to camera noise. Highly absorptive materials restrict the amount of light back-scattered after undergoing multiple scattering, leading to a higher speckle contrast, which affects the autocorrelation function for data collected without a polarizer. Wood and brown carton are more absorptive than white paint and paper, and therefore their autocorrelation peaks are taller for the data collected without a polarizer [Fig. 3(b)]. All autocorrelations measured fit Gaussian

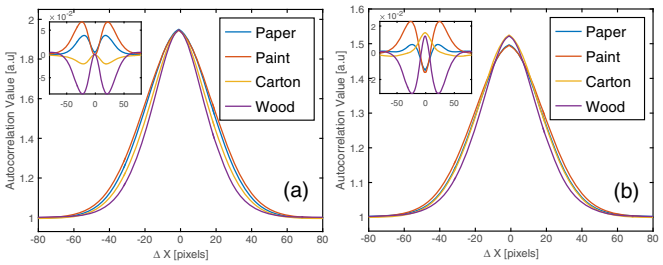

Fig. 3. Cross sections of the normalized autocorrelation functions. $\Gamma_I(\Delta x, \Delta y; \Delta y = 0)$ of speckles from four different materials averaged over 180 images. (a) Polarizer perpendicular to the illumination polarization; (b) no polarizer. Graphs of the difference between each material and the average of all four are presented in the upper left corners.

functions ($R > 0.98$), slightly overvalued near the center and undervalued towards the tails. We believe that the differences in both the widths and shapes of these measured autocorrelations are the result of the different amounts of beam smearing that occurred within the thick diffusers due to volumetric scattering. Had the materials' surface been dictating the autocorrelation's shape, this effect would not have shown up in the images collected in the polarization perpendicular to the laser's polarization [Fig. 3(a)]. We note that we are sampling only a small section of the speckle pattern, and the speckle intensity is practically uniform over this region.

We found that using the power spectral density function G_I rather than the autocorrelations gave slightly better results. Moreover, using the log of G_I further improved our algorithm's predictive rate probably due to its sensitivity to the wings of G_I. We calculated several statistical parameters for each speckle pattern: the contrast, several moments of the log of G_I, and a few more that proved to be less effective (detailed in Supplement 1). These parameters formed the parameter vector representing the speckle pattern created from a specific point of a given material.

When comparing the results of the CNN versus LDA algorithms (Fig. 2), we find similar results with a slight edge to the LDA algorithm. This is probably due to the CNN algorithm being given only small parts of the original speckle images in order to save analysis time (details in Supplement 1). We expect the CNN predictive rate to surpass its LDA counterpart, had full sized images been used and the neural network been fine tuned.

For every material set, collecting data in different polarizations proved to give slightly different predictive rates (Fig. 2). Light scattered from a surface contains only the polarization parallel to the illumination's polarization, yet light that underwent multiple scattering is roughly unpolarized. Therefore, the algorithm's success when given speckles observed in the polarization perpendicular to the laser's polarization attests to the claim that the volumetric scattering is causing the identifiable changes in the speckles created. On the other hand, the paint samples created using the same white paint, but dried with different surface roughnesses, were also successfully classified by the algorithm, suggesting the scatterer's surface affects the speckles created as well. Moreover, on the measurements done on these paint samples, the data collected in the polarization parallel to the laser's polarization gave the best predictive results. This is probably due to the difference in the samples being mostly related to their surfaces. By filtering out the light in the perpendicular polarization, only the light that contains this difference is collected. In addition, materials with higher absorption coefficients emit less multiple scattered light, and therefore create higher-contrast speckle

patterns. This contrast difference can only be observed in images acquired with no polarizer, which gave the best results for the wood material set.

Our method achieved different levels of success depending on the data sets (the material sets observed in a specific polarization) being compared. For both algorithms, the total number of images used per data set (specific sample and polarization) was $N = 180$. The algorithms then split each data set into a training set, which gives the algorithms their recognition capabilities, and a test set, used to check their acquired predictive accuracy. The training sets were composed of 90% of the total data for the CNN algorithm and 66% for the LDA algorithm. The algorithms' predictive accuracy improved for the following circumstances: decreasing the number of materials being compared (M), increasing the number of images acquired for every sample (N), and checking materials with increasingly different scattering parameters.

In order to improve the predictive accuracy, one can use several speckle images (n) from a single unknown sample instead of the single-shot method presented earlier. This is useful for distinguishing between very similar scatterers, such as the white papers created by two different manufacturers (Fig. 2). While the single-shot, no-polarizer mode gave us less than 80% probability to identify the manufacturer correctly, using numerous images greatly improved the results (Fig. 4). When using $n = 10$ images, our LDA algorithm correctly predicted the sample creating the speckle patterns with 98% accuracy.

In order to check the robustness of our system, we scanned some samples several times on different days to verify that the statistical parameters we measured remained consistent. We then checked that when changing the camera's shutter time and receiving reasonably small changes in the images' mean intensity (~5%); the algorithm cannot differentiate between the sample's new data and its previously compiled data. This assured our notion that the temperature, humidity, laser mode, and the camera's shutter time were not causing the statistical deviations we were picking up on.

By looking at speckles created via transmission, we verified that the polarization ratio rises with a material's thickness in scales similar to the penetration depth. The speckle statistics changed sharply with the material thickness, thus allowing us to use the same LDA algorithm in order to optically recognize the material's thickness for a known substance (detailed in Supplement 1).

In summary, we have experimentally demonstrated that a speckle pattern contains information about the scatterer used to create it.

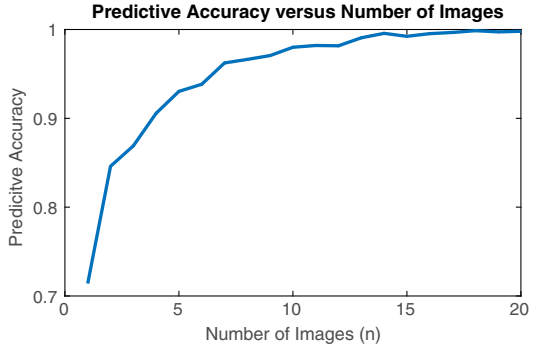

Fig. 4. Differentiating between two white papers created by different manufacturers by inserting multiple images of their speckles into the LDA algorithm.

We found that this information can be used to classify different scattering samples and could possibly be used to learn about both the sample's surface and its volumetric scattering parameters. Further research is necessary to find the relation between the statistics of a speckle pattern and the features of the object creating it.

Our technique proved successful in single-shot scatterer recognition for data sets containing several materials in either bulk or powder form. We have demonstrated the ability to differentiate between materials with either surface or substance dissimilarities, even when using slightly noisy data. In addition, when using data from multiple scanned points, our method can be used to identify exceedingly similar materials. These abilities can be further improved by using better algorithms or measuring additional data, and the capabilities can most likely be expanded to scattering liquids by using a pulsed narrowband laser. Furthermore, by rotating the camera position around a material and repeating this process for many angles, the small features of the scatterer can be expressed through the large features of the speckle pattern. This could potentially improve the results drastically and be used to learn about the scatterers' microscopic features. There is no theoretical reason to assume the uniqueness of a material's speckle pattern, yet this method may prove to be sufficient for differentiating one material sample from a limited set of others or as an additional measurement to existing means of material recognition.

Funding. Israeli Centers for Research Excellence (I-CORE); Israeli Ministry of Science (712845); Crown Photonics Center.

Acknowledgment. We thank Dekel Ra'anan and Ronen Chriki for their fruitful insights and Nitzan Artzi for his help with the learning algorithms.

Coding for the CNN algorithm, speckle image parameters, and LDA algorithm are available at Code 1, Ref. [12], Code 2, Ref. [13], and Code 3, Ref. [14], respectively.

See Supplement 1 for supporting content.

REFERENCES

1. J. W. Goodman, *Speckle Phenomena in Optics: Theory and Applications* (Roberts & Company, 2007).
2. C. Dainty, E. Ennos, M. Francon, J. Goodman, S. McKenchnie, and G. Parry, *Laser Speckle and Related Phenomena* (Springer, 1975).
3. J. S. Lee, L. Jurkevich, P. Dewaele, P. Wambacq, and A. Oosterlinck, Remote Sens. Rev. **8**, 313 (1994).
4. R. Erf, *Speckle Metrology* (Elsevier, 2012).
5. O. Katz, P. Heidmann, M. Fink, and S. Gigan, Nat. Photonics **8**, 784 (2014).
6. J. Leendertz, J. Phys. E **3**, 214 (1970).
7. G. Danuser and C. Waterman-Storer, Annu. Rev. Biophys. Biomol. Struct. **35**, 361 (2006).
8. W. B. Ribbens, Appl. Opt. **8**, 2173 (1969).
9. F. Luk, V. Huynh, and W. North, J. Phys. E **22**, 977 (1989).
10. M. Egmont-Petersena, D. Ridderb, and H. Handelsc, Pattern Recognit. **35**, 2279 (2002).
11. G. McLachlan, *Discriminant Analysis and Statistical Pattern Recognition* (Wiley, 2004).
12. CNN to predict materials from their corresponding speckles, https://doi.org/10.6084/m9.figshare.5777598.
13. Parameter vectors from speckle images, https://doi.org/10.6084/m9.figshare.5777595.
14. LDA to predict materials from their corresponding parameter vectors, https://doi.org/10.6084/m9.figshare.5777601.